Integrating Coot Optimization Algorithm with Deep Learning based Medical Image Analysis for Pancreatic Cancer Diagnosis

Eiman Talal Alharby[1,*]

[1]Department of Computer Science and Artificial Intelligence, College of Computing, Umm Al-Qura University, Makkah, Saudi Arabia

Email: Etharby@uqu.edu.sa

Abstract

Pancreatic cancer (PC) is an extremely malignant cancer type with a maximum rate of mortality. It remains a challenging form of tumor to treat due to its late analysis and aggressive nature, which drastically decreases the survival rate. Early analysis of PC is vital for enhancing the probabilities of treatment and survival. PC analysis was initially dependent upon imaging, and then the recent imaging offered a worse prognosis, restraining clinicians' treatment choices. PC detection utilizing deep learning (DL) contains the application of advanced computational methods for analyzing medical image data like CT scans or MRI images, for the early and correct detection of PCs. DL approaches, particularly convolutional neural networks (CNNs), are trained on huge databases for diagnosing forms and anomalies indicative of PC. Therefore, this study presents a novel Coot Optimization Algorithm with Deep Learning based Medical Image Analysis for Pancreatic Cancer Diagnosis (COADL-MIAPCD) technique. The main objective of the COADL-MIAPCD approach is to proficiently examine the medical images for the detection of PC. The COADL-MIAPCD technique primarily applies a median filtering (MF) for image pre-processing. In addition, the COADL-MIAPCD approach allowed using of an improved SE-ResNet. Moreover, the COA has been utilized for the optimum parameter choice of the improved SE-ResNet. At last, the extreme learning machine (ELM) has been used for the recognition and classification of PCs. The simulation outcomes of the COADL-MIAPCD technique has been validated utilizing a medical image database. The obtained experimental values stated that COADL-MIAPCD technique achieves better performance than other models.

Keywords: Pancreatic Cancer; Medical Image; Deep Learning; Coot Optimization Algorithm; Computed Tomography

1. Introduction

Pancreatic cancer (PC) has become the fourth most widespread reason of cancer-specific mortality around the world, with an occurrence rate equivalent to its mortality rate [1]. While there are tremendous evolutions in the earlier identification and treatment of distinct malignancies like prostate cancer, breast cancer (BC), and colorectal cancer, the prediction of PC is complicated, as the five-year survival rate can be smaller than 5% and its mortality rate will not be decreased during recent years [2]. Then, PC appears to endure major significant issues in the combat against malignancy in the 21st century. The most prevalent reason for the ineffective analysis of PC is the complexity of its earlier analysis. Although several problems are detailed above, there will be a continual effort to accomplish earlier detection and make the suitable choice of medical candidates with PC [3]. Recently, accessible pancreatic imaging techniques have a main role in the representation of surgical and treatment development, initial phases, pancreatic focal lesions, and evaluation of the treatment responses employing diverse imaging techniques comprising endoscopic ultrasonography (EUS), CT, MRI, ultrasonography (US), and positron emission tomography (PET). Multi-detector row CT (MDCT) is a crucial part of the analysis and phases of pancreatic malignancies [4].

In recent years, developments in computer technology have been seen, combined with the improvement of efficient image processing approaches, which can be conducted in the new years of 'digital medicine' [5]. Accordingly,

DOI: https://doi.org/10.54216/FPA.190119
Received: November 02, 2024 Revised: January 09, 2025 Accepted: February 05, 2025

medical practitioners can prevent the difficult medical image analysis achieved manually, therefore, addressing errors and saving time in analysis occurring, because of the variances in proficiency and medical experience. The 21st century was perceived as the extensive usage of artificial intelligence (AI) that implements computer techniques for executing activities related to human intelligence, like problem solving and learning. In the mid-1950s, the words 'AI' were initially introduced by John McCarthy, and developed in a group of 'if-then' commands to additional intricate methods that imitate the human brain in a few characteristics [6]. The utilization of AI tools provides the development of an innovative domain of medical analysis such as accurate oncology that employs a huge quantity of data from metabolomics, proteomics, and genomics. ML employs computational techniques for analysing massive amounts of information and recognizing the patterns for prediction [7]. ML will be supervised wherein it utilizes data from prior experiments or assessments to recognize the models or tendencies to create predictions [8]. During the diagnosis of PC, CT, PET scans, MRI, and US data should be employed for training the model to recognize abnormalities that will be categorized as PC [9]. The accuracy of the prediction must be better once huge amounts of data have been employed for the training. ML is also unsupervised wherein it will differentiate the patterns and trends in uncategorized data. However, the predictive accuracy will be moderately compromised by comparison with the supervised techniques [10]. The 3D renovation of images is accomplished by the ML methods for higher diagnostic accuracy.

This study offers a novel Coot Optimization Algorithm with DL-based Medical Image Analysis for PC Diagnosis (COADL-MIAPCD) technique. The main intention of the COADL-MIAPCD approach is to proficiently examine the medical images for the PC detection. The COADL-MIAPCD technique primarily applies a median filtering (MF) for image pre-processing. In addition, the COADL-MIAPCD approach allowed using of an improved SE-ResNet algorithm. Moreover, the COA has been utilized for the optimum parameter choice of the improved SE-ResNet. At last, the extreme learning machine (ELM) has been used for the detection and classification of PCs. The simulation results of the COADL-MIAPCD has been validated using a medical image database.

2. Literature Works

Yang et al. [11] presented a DL-based technique for pancreas segmentation. This method employed a 3D nnU-net model for segmentation. Moreover, consensus segmentation has been acquired by employing the STAPLE method. Afterward, the pancreases capacities identified by automated segmentation have been related to manual segmentation. The authors [12] developed an intelligent DL-assisted decision-making medical system for pancreatic tumour classification (IDLDMS-PTC) technique. This system obtains an EPO with a multilevel threshold (EPO-MLT) algorithm for segmenting PCs. The multileader optimization (MLO) method must be also deployed. Ramesh et al. [13] aimed to an innovative SSA with stacked-based Medical Image Analysis for PC Detection and Classification (SSASDL-PCDC) method. This method implements HHO with a DenseNet system in the feature extraction method. Additionally, the CNN-BiLSTM technique has been employed to identify and classify the PC. Moreover, SSA should be employed for modifying the hyperparameter values.

Laxminarayanamma et al. [14] considered the smaller lesions and introduced a novel, effective, and automatic DL network system for PDAC identification. The Improved Deep Residual CNN (IDRCNN) method identifies the PDAC. The hyperparameter was employed by applying the TSOA. An improved analysis must be gained owing to segmenting the nearby anatomy structure impact like PD. Paithane and Kakarwal [15] projected an LMNS-net DL, bottom-up method. For the segmentation of the serious pancreas employing numerous viewpoints of CT scans like sagittal, axial, and coronal, a developed LMNS-net architecture was employed. At the LMNS-Net system, 12 layers have been utilized with 4 convolution layers. This technique was utilized for several organ segmentations. The lightweight multiscale block was employed in a method that could be integrated with the essential feature only thereby unemployed data failure in the convolution layer. Zhang et al. [16] developed an instance-aware technique that improves the ViT with an innovative shuffle instance strategy (SI-ViT) technique. This method introduces a shuffle stage for producing bags of SI and consistent bag-level soft labels, permitting the system to comprehend associations and allocations more than the restricted new allocations. Meanwhile, integrated with a un-shuffle stage, the conventional ViT will make the connections with respect to the instance labels.

Lakkshmanan and Ananth [17] examined an innovative DL method. Mainly, a BF algorithm was implemented for image preprocessing. Moreover, the non-interactive GrabCut (NIGC) method was employed for segmentation. Then, ResNet152 architecture was employed as a feature extractor. Lastly, the RDA-tuned BPNN named as RDA-BPNN system can be utilized as a classification technique. Qin et al. [18] designed hyperspectral imaging (HSI) enabled CNN method to support the analysis of pancreatic EUS-FNA cytology samples. A CNN has been recognized to examine the diagnosis efficiency, and Attribution Guided Factorization Visualization (AGF-Visualization) has been deployed for visualizing the field of significant classification features recognized through the system.

DOI: https://doi.org/10.54216/FPA.190119
Received: November 02, 2024 Revised: January 09, 2025 Accepted: February 05, 2025

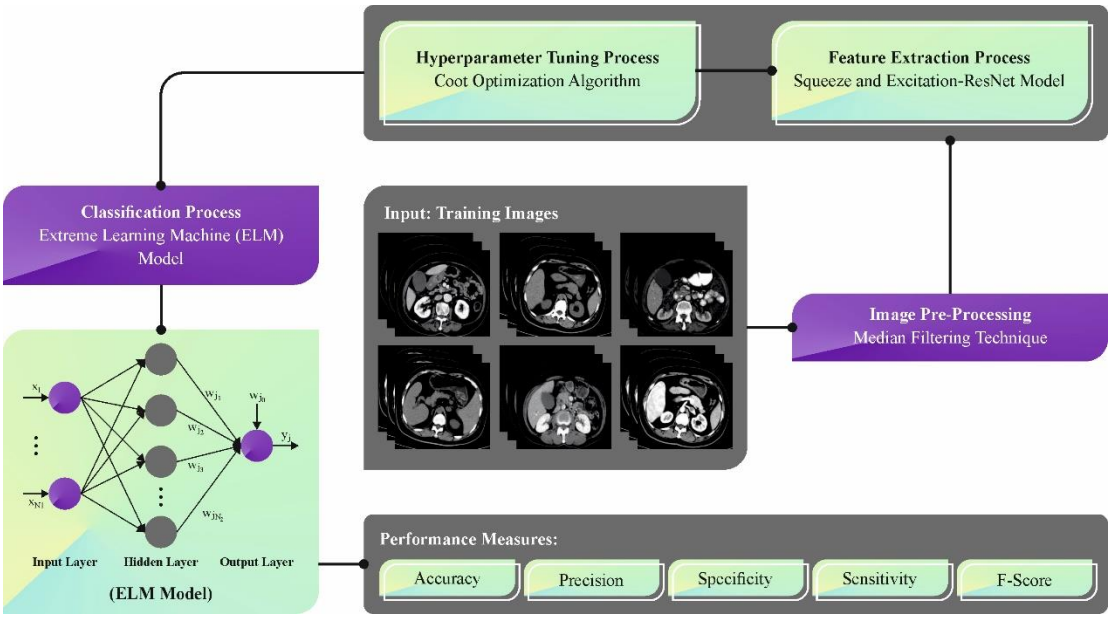

Figure 1. Overall flow of COADL-MIAPCD technique

3. The Proposed Model

This study presented a novel COADL-MIAPCD methodology. The main intention of the COADL-MIAPCD approach is to proficiently examine the medical images for the identification of the PC. Fig. 1 exemplifies the entire flow of the COADL-MIAPCD methodology.

A. Image Preprocessing

Primarily, the COADL-MIAPCD approach applies the MF approach for image pre-processing. MF is a popular image preprocessing approach deployed to decrease noise and improve the entire digital image quality [19]. This approach involves sliding a window over the image pixel by pixel and replacing every pixel intensity values with the median rate of the nearby pixels within the determined window. Distinct mean filter that computes the average, MF is robust to outliers and maintains edges and fine details from the image. This makes it mainly effective in suppressing salt-and-pepper noise, a kind of random, isolated pixel noise generally found in images attained from distinct sources namely medical imaging or low-light photography. MF was extremely employed in various apps but noise reduction is vital for enhancing image clarity and analysis.

B. Feature Extraction

The COADL-MIAPCD system allowed using of an improved SE-ResNet algorithm to learn complex and intrinsic feature patterns. Hu et al. introduced SE-Net, which carries out feature recalibration across the network, whereby it learns to use data globally to suppress less relevant features and to selectively emphasize relevant features [20]. The Squeeze function compresses the 2D feature maps of the mapping feature U alongside the channel direction into real numbers to create it 1x1xc_2 mapping feature, and exploits the global average pooling model for compressing the mapping feature$U$ alongside the spatial size:

$$Z_c = F_{sq}(u_c) = \frac{1}{W \times H}\sum_{i=1}^{n}\sum_{i=1}^{n} u_c\,(i,j) \tag{1}$$

In Eq. (1), W, H, C indicate the three dimensions to extract the feature maps, and the squeeze function is represented by F_{sq}. The excitation function presents the parameter W to 1×1×c_2 mapping feature attained by the squeeze function and assigning respective weights based on the impact of the feature channel:

$$s = F_{ex}(z, W) = \sigma\big(g(z, W)\big) = \sigma\big(W_2\delta(W_1 z)\big), \tag{2}$$

In Eq. (2), the excitation operation is denoted by F_{ex}, and the outcome of squeeze function is z, $W_1 \in R^{\frac{c}{r}\times C}$, $W_2 \in R^{C\times\frac{c}{r}}$. The reweight function used to load the weight attained by the Excitation function, viz., the significance of feature channels into the new feature channels:

$$\tilde{x}_c = F_{scale}(u_c, s_c) = s_c \cdot u_c, \tag{3}$$

DOI: https://doi.org/10.54216/FPA.190119
Received: November 02, 2024 Revised: January 09, 2025 Accepted: February 05, 2025

In Eq. (3), the reweight operation is indicated as F_{scale}.

The bottleneck structure of 1×1, 3×3, 3×3 and the basic structure of 1×1, 3×3 convolutions are the two different structures of the ResNet block, both networks are embedded in SE-Net:

The number of CNN parameters becomes huge due to the continuous model deepening that result in over-fitting. Over-fitting is a phenomenon where the generalization performance is poor and the loss function is very small. Simultaneously, the increase in the parameter number decreases the training efficacy, increases the computation, and increases memory consumption. We can achieve the popularization and promotion of DL techniques only by decreasing the parameter number in conjunction with the effective computational power of GPU. Hence, another solution is to decrease the parameter number of the CNN except for data enhancement of the training set. It changes the new ResNet block to small module with 1×3, 3×1, 1×3, and 3×1 structures. Fig. 2 reveals the structure of SE-ResNet model.

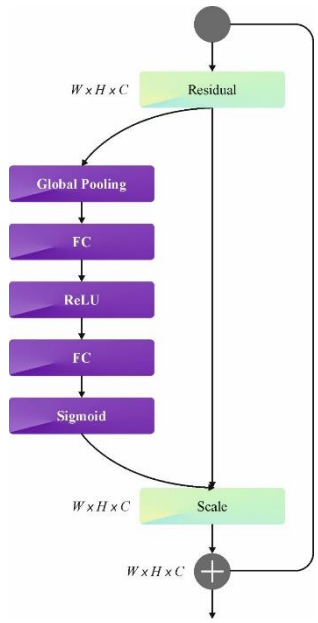

Figure 2. Structure of SE-ResNet

Eq. (4) is used to compute the parameters of the convolution layer.

$$T_{conv} = C \times H \times W \times K, \tag{4}$$

Where K refers to the amount of convolutional kernel and $C \times H \times W$ denotes the dimensional of the convolutional kernel.

$$T_{basic} = (64 \times 3 \times 3 \times 64) \times 2 = 18 \times 64^2 \tag{5}$$

$$T_{bottleneck} = 256 \times 1 \times 1 \times 64 + 64 \times 3 \times 3 \times 64 \tag{6}$$
$$+64 \times 1 \times 1 \times 256 = 17 \times 64^2$$

$$T_{small} = (64 \times 1 \times 3 \times 64) \times 2 \tag{7}$$
$$+(64 \times 3 \times 1 \times 64) \times 2 = 12 \times 64^2.$$

This structure decreased the parameter number more than the basic and bottleneck structures where the training efficiency improved and the ability of feature extraction remained the same.

C. COA-based Parameter Tuning Process

Next, the COA has been employed for the optimal parameter choice of the improved SE-ResNet. The COOT approach was introduced by Iraj Naruei, which becomes a newly presented metaheuristic optimizer method that targets to imitate the cooperative behavior of a group of coot birds [21]. When compared to alternative optimizer techniques, comprising the PSO algorithm and the discrepancy evolution technique, the COOT technique has fast convergence velocity and higher accuracy in convergence. Furthermore, the COOT technique is undertaking validation at some engineering applications, comprising welded beam design, pressure vessel design, rolling

DOI: https://doi.org/10.54216/FPA.190119
Received: November 02, 2024 Revised: January 09, 2025 Accepted: February 05, 2025

bearing, and stepped cone pulley complexities. The fundamental notion of the COOT technique will be explained as follows.

(1) The primary assignment of the coot population can be demonstrated and then the calculation of the related fitness levels for all the populations.

$$Q = Lb + rand(1, d) * (Ub - Lb) \tag{8}$$

Now, d refers to the size of the problem that should be resolved, Q was made by the method of arbitrarily initializing the population. Furthermore, the Ub and Lb denote the upper and lower boundaries of the population locations. The matrix exhibiting the locations of the coot can be determined as represented in this formula.

$$Cpos^{l} = [x_{N,1}^{l}, x_{N,D}^{l}, .., x_{N,D}^{l}] \tag{9}$$

Now, $Cpos^{l}$ refers to the whole coot location, and N signifies the population's scale.

$$Fit^{l} = [fit_{1}^{l}, fit_{2}^{l}, .., fit_{N}^{l}] \tag{10}$$

Now, fit_{i}^{l} describes the fitness rate of i_{th} individual simultaneously l_{th} iteration.

(2) General coot population position upgrade

The existing movement of the coot was demonstrated by imitating the cooperative movement of the population dependent upon the different cooperative ways demonstrated by the leader and distinctive coot individual. Therefore, it has four various models of movements noticed on the surface of the water chain movement, random movement, movements directed by the leader of the overall population.

A position is produced arbitrarily inside the spatial domain, permitting a collective one to later upgrade the position. This mathematical equation leading to the unintended mobility of the individual will be given as follows:

$$Cpos(i) = Cpos(i) + A \times R2 \times \big(Q - Cpos(i)\big) \tag{11}$$

Whereas A denotes a reducing integer level from 0 to 1, the position of the i_{th} the distinctive individual is signified as $Cpos(i)$, $R2$ shows an unintended value among zero and one, and Q specifies a random allocation inside the search area. The subsequent formula calculates the values of A and Q as indicated below:

$$\begin{cases} A = 1 - \dfrac{l}{L} \\ Q = rand(1, d) * (UB - LB) + LB \end{cases} \tag{12}$$

Now, L describes the iteration's highest number to be executed and l indicates the iteration's existing number correspondingly.

A distance vector between 2 individuals upgrades the position across the distinctive population chain action. The computational equation for the chain can be defined as follows:

$$Cpos(i) = 0.5 \times \big(Cpos(i-1) + Cpos(i)\big) \tag{13}$$

In the condition of leader-based position alteration, the distinctive individual will need to adapt their position through the k_{th} leader

$$Cpos(i) = Lpos(k) + 2 \times R1 \times \cos(2R\pi) \times \big(Lpos(k) - Cpos(i)\big) \tag{14}$$

Now, $Lpos(k)$ defines the k_{th} leader's position, $R1$ refers to an accidental integer with the level zero and one, and k variable was chosen as shown:

$$k = 1 + (iMODm) \tag{15}$$

From this mathematical formula, i denotes the existing member of the i_{th} coot swarm and m indicates the total no. of leaders.

(3) Position upgrade of the leader population

In a component of leader's position change, it will not be exceptional for the leader to step down from the presently optimum position to assist in the detection of a place to be more beneficial. The next summarizes the position of leaders,

$$Lpos(i+1) = \begin{cases} B \times R3 \times \cos(2R\pi) \times \big(gbest - Lpos(i)\big) + gbestR4 < 0.5 \\ B \times R3 \times \cos(2R\pi) \times \big(gbest - Lpos(i)\big) - gbestR4 \geq 0.5 \end{cases} \tag{16}$$

DOI: https://doi.org/10.54216/FPA.190119
Received: November 02, 2024 Revised: January 09, 2025 Accepted: February 05, 2025

Here, $gbest$ specifies the existing constant position, $R3$, and $R4$ variables signify accidental values within the level of 0 to 1 and then, this adapted location of variable B is drawn as follows:

$$B = 2 - \frac{l}{L} \tag{17}$$

The COA is an FF to complete higher classifier solutions. It describes a positive integer to exemplify the optimum result of candidate results.

$$fitness(x_i) = ClassifierErrorRate(x_i)$$
$$= \frac{No.of\ misclassified\ instances}{Total\ no.of\ instances} * 100 \tag{18}$$

D. Cancer Detection using ELM Model

At last, the ELM model is deployed for the detection and classification of PCs. Huang et al. introduced ELM to decrease the cost of training time the iterative parameter-tuning model [22]. It is a feedforward NN with a single hidden layer (HL), input, and output layers. It can achieve low training errors. Since the ELM model is direct and does not need any iterative parameter tuning, then the training model is boosted. It contains 500 hidden nodes, 5 output nodes, and 100 input nodes for the multi-class classification, and, there is 1 output node rather than 5 for binary classification. Assume a DR training sample as $\{X_1, Y_1\} = \{x_{(1,m)}, y_{(1,t)} : m\epsilon R+, t\epsilon R+\}$. X is the input, and Y is the output. The training sample is formulated by:

$$X_{(n,m)} = \begin{bmatrix} x_{(1,1)} & x_{(1,2)} & \cdots & x_{(1,m)} \\ x_{(2,1)} & x_{(2,2)} & \cdots & x_{(1,m)} \\ x_{(3,1)} & x_{(3,2)} & \cdots & x_{(1,m)} \\ \vdots & \vdots & & \vdots \\ x_{(n,1)} & x_{(n,2)} & \cdots & x_{(n,m)} \end{bmatrix} \tag{19}$$

$$Y_{(n,t)} = \begin{bmatrix} y_{(1,1)} & y_{(1,2)} & \cdots & y_{(1,t)} \\ y_{(2,1)} & y_{(2,2)} & \cdots & y_{(1,t)} \\ y_{(3,1)} & y_{(3,2)} & \cdots & y_{(1,t)} \\ \vdots & \vdots & & \vdots \\ y_{(n,1)} & y_{(n,2)} & \cdots & y_{(n,t)} \end{bmatrix} \tag{20}$$

Here n signifies the instance counts, m implies the attribute counts, and t indicates the amount of output nodes. Where $m = 100$ and the value of n are different with the size of the training and testing set. For multi-class classification $t = 5$ and binary class $t = 1$. The N implies the count of hidden nodes, the value of N will be 500, input weighted $W(m, N)$, and bias $B(1, N)$ matrices are randomly produced.

$$W_{(m,N)} = \begin{bmatrix} w_{(1,1)} & w_{(1,2)} & \cdots & w_{(1,N)} \\ w_{(2,1)} & w_{(2,2)} & \cdots & w_{(1,N)} \\ w_{(3,1)} & w_{(3,2)} & \cdots & w_{(1,N)} \\ \vdots & \vdots & & \vdots \\ w_{(m,1)} & w_{(m,2)} & \cdots & w_{(m,N)} \end{bmatrix} \tag{21}$$

$$B(1, N) = [b_{(1,1)}\ b_{(1,2)} \ldots\ b_{(1,N)}]$$

The resultant of the HL is calculated by

$$H_{(n,N)} = G\left(X_{(n,m)} \cdot W_{(m,N)} + B_{(1,N)}\right). \tag{22}$$

Here $G(x)$ shows the activation function.

$$H_{(n,N)} = \begin{bmatrix} h_{(1,1)} & h_{(1,2)} & \cdots & h_{(1,N)} \\ h_{(2,1)} & h_{(2,2)} & \cdots & h_{(1,N)} \\ h_{(3,1)} & h_{(3,2)} & \cdots & h_{(1,N)} \\ \vdots & \vdots & & \vdots \\ h_{(m,1)} & h_{(m,2)} & \cdots & h_{(n,N)} \end{bmatrix} \tag{23}$$

By using the Moore-Penrose pseudo inverse, the output layer weight $\beta_{(N,t)}$ is calculated:

$$\beta_{(N,t)} = H^{\dagger}_{(N,n)} \cdot T_{(n,t)} \tag{24}$$

t =number of outputs

T =Output of the training set

DOI: https://doi.org/10.54216/FPA.190119
Received: November 02, 2024 Revised: January 09, 2025 Accepted: February 05, 2025

4. Experimental Validation

The performance validation of the COADL-MIAPCD method occurs using a medical image dataset comprising 500 instances and 2 classes as reported in Table 1.

Table 1: Details of the dataset

Classes	No. of Instances
"Pancreatic Tumor"	250
"Non-Pancreatic Tumor"	250
Total Instances	500

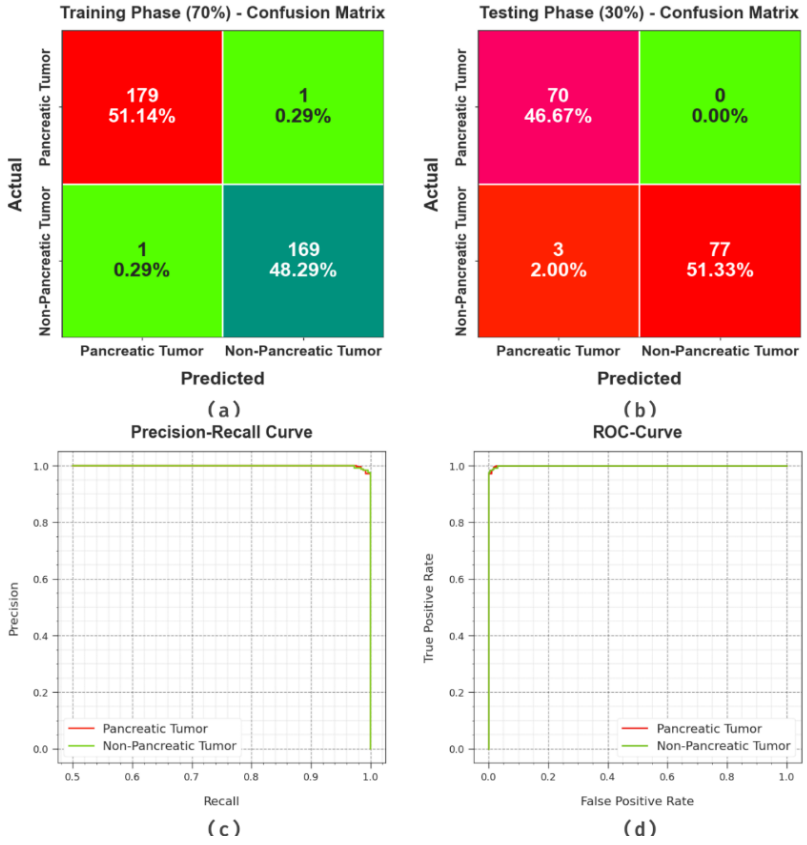

Figure 3. (a-b) 70%TRAPA:30%TESPA (c-d) PR-Curve and ROC-Curve

Fig. 3 shows the classifier outcomes of the COADL-MIAPCD at test database. Figs. 3a-3b describes the confusion matrices offered by the COADL-MIAPCD technique on 70%TRAPA:30%TESPA. This outcome signified that the COADL-MIAPCD algorithm has correctly identified and considered pancreatic and non-pancreatic tumors class labels. Additionally, Fig. 3c highlights the PR outcome of the COADL-MIAPCD algorithm. The outcome reported that the COADL-MIAPCD gains excellent PR effectiveness in all classes. In conclusion, Fig. 3d exemplifies the ROC result of the COADL-MIAPCD. The outcome stated that the COADL-MIAPCD offers effectual solutions with improved values of ROC on 2 classes.

In Table 2 and Fig. 4, the cancer detection results of the COADL-MIAPCD at 70%TRAPA:30%TESPA are clearly demonstrated. These experimental values show that the COADL-MIAPCD technique reaches effectual identification of class labels. On 70%TRAPA, the COADL-MIAPCD attains an average $accu_y$ of 99.43%, $prec_n$ of 99.43%, $sens_y$ of 99.43%, $spec_y$ of 99.43%, and F_{score} of 99.43%. Meanwhile, based on 30%TESPA, the COADL-MIAPCD offers an average $accu_y$ of 98.12%, $prec_n$ of 97.95%, $sens_y$ of 98.12%, $spec_y$ of 98.12%, and F_{score} of 98%.

DOI: https://doi.org/10.54216/FPA.190119
Received: November 02, 2024 Revised: January 09, 2025 Accepted: February 05, 2025

Table 2: Cancer detection of the COADL-MIAPCD at 70%TRAPA:30%TESPA

Class	$Accu_y$	$Prec_n$	$Sens_y$	$Spec_y$	F_{score}
TRAPA (70%)					
Pancreatic Tumor	99.44	99.44	99.44	99.41	99.44
Non-Pancreatic Tumor	99.41	99.41	99.41	99.44	99.41
Average	99.43	99.43	99.43	99.43	99.43
TESPA (30%)					
Pancreatic Tumor	100.00	95.89	100.00	96.25	97.90
Non-Pancreatic Tumor	96.25	100.00	96.25	100.00	98.09
Average	98.12	97.95	98.12	98.12	98.00

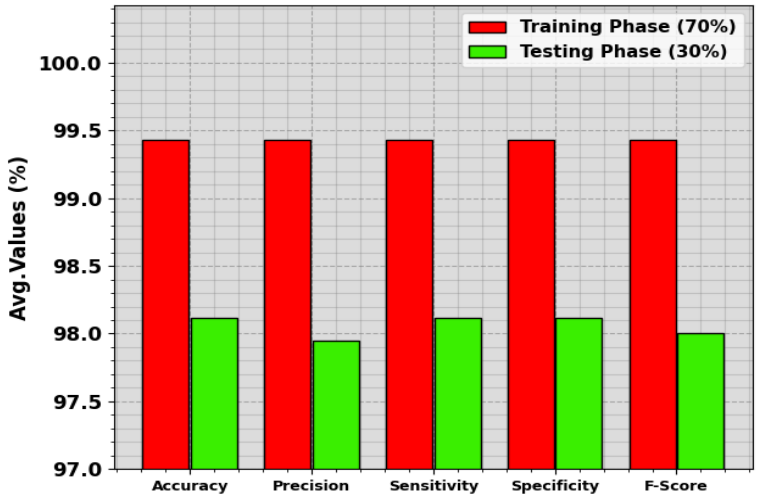

Figure 4. Average of the COADL-MIAPCD system on 70%TRAPA:30%TESPA

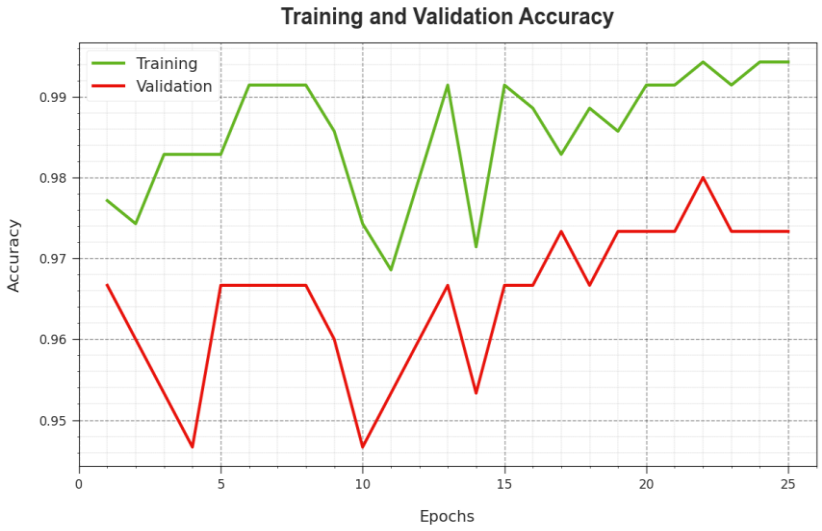

Figure 5. $Accu_y$ Curve of the COADL-MIAPCD model

DOI: https://doi.org/10.54216/FPA.190119
Received: November 02, 2024 Revised: January 09, 2025 Accepted: February 05, 2025

The efficacy of the COADL-MIAPCD is clearly demonstrated in Fig. 5 in the form of training $accu_y$ (TRAAC) and validation $accu_y$ (VALAC) curves. This outcome exhibits a valuable outcome of the behaviour of the COADL-MIAPCD technique over changing epoch counts, representing its learning model and generalized abilities. The increased trends in VALA outline the ability of the COADL-MIAPCD to adjust and besides to offer correct classification of unnoticed information, implied that the robust generalized capabilities.

Fig. 6 displays a comprehensive illustration of the TRA loss (TRALO) and VAL loss (VALLO) outcomes of the COADL-MIAPCD technique over various epochs. The progressive minimizes in TRLA highpoints the COADL-MIAPCD increasing the weights and minimizing the classifier error on the two data. The outcome point out a perfect accepting of the COADL-MIAPCD algorithm appropriate to TRA, emphasizing its ability in capturing designs.

Figure 6. Loss curve of the COADL-MIAPCD technique

Table 3 demonstrated the outcomes of the COADL-MIAPCD methodology and compared methods [13].

Table 3: Comparative outcome of the COADL-MIAPCD with other systems

Methods	$Sens_y$	$Spec_y$	$Accu_y$
COADL-MIAPCD	99.43	99.43	99.43
SSASDL-PCDC	99.26	99.26	99.26
IDLDMS-PTC	99.05	98.84	99.15
ODL-PTNTC	98.73	97.75	98.40
WELM Algorithm	97.76	97.67	97.26
KELM Techniques	96.66	97.53	96.69
ELM Techniques	96.27	97.27	96.21
CNN Algorithm	91.50	86.70	87.40

In Fig. 7, the comparative values of the COADL-MIAPCD technique with respect to $accu_y$ are portrayed. The figure indicate that the CNN method demonstrates poor performance with least value of $accu_y$. Meanwhile, the ODL-PTNTC, KELM, WELM, and ELM techniques have managed to report considerable $accu_y$ values. Although the SSASDL-PCDC and IDLDMS-PTC algorithms have revealed reasonable $accu_y$ values, the COADL-MIAPCD algorithm establishes higher outcome with a maximal $accu_y$ of 99.43%.

DOI: https://doi.org/10.54216/FPA.190119
Received: November 02, 2024 Revised: January 09, 2025 Accepted: February 05, 2025

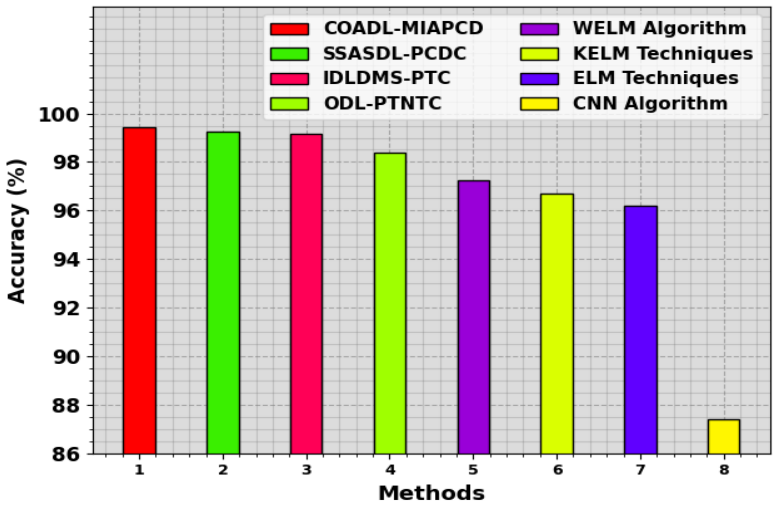

Figure 7. $Accu_y$ Result of the COADL-MIAPCD with other algorithms

A comparative calculation of the COADL-MIAPCD with respect to $sens_y$, and $spec_y$ can be reported in Fig. 8. The outcome implies that the CNN technique determines poorer outcome with the minimal values of $sens_y$ and$spec_y$. Similarly, the ODL-PTNTC, KELM, WELM, and ELM systems are acquired to provide considerable$sens_y$, and $spec_y$ values. While the SSASDL-PCDC and IDLDMS-PTC algorithms have discovered considerable $sens_y$ and $spec_y$values, the COADL-MIAPCD method indicates greater performance with increased$sens_y$, and $spec_y$ of 99.43% and 99.43%, respectively.

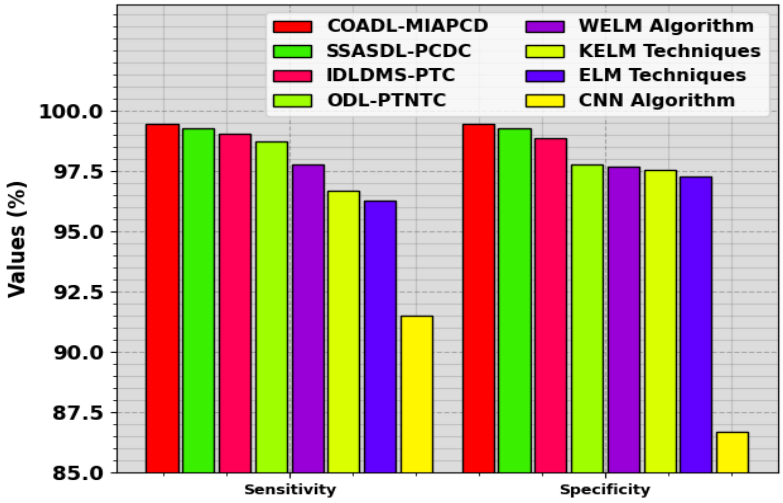

Figure 8. $Sens_y$, and $Spec_y$ result of the COADL-MIAPCD model with recent approaches

Table 4: CT outcome of the COADL-MIAPCD with other algorithms

Methods	Computational Time (sec)
COADL-MIAPCD	0.51
SSASDL-PCDC	0.88
IDLDMS-PTC	1.02
ODL-PTNTC	1.37

DOI: https://doi.org/10.54216/FPA.190119
Received: November 02, 2024 Revised: January 09, 2025 Accepted: February 05, 2025

WELM Algorithm	1.35
KELM Techniques	1.37
ELM Techniques	1.38
CNN Algorithm	1.48

A wide-ranging computational time (CT) comparative outcome of the COADL-MIAPCD technique has been examined in Table 4 and Fig. 9. This figure displays that the CNN system exhibits ineffectual performance with the boosted value of CT. Moreover, the ODL-PTNTC, KELM, WELM, and ELM systems are achieved as moderated CT values. However, the SSASDL-PCDC and IDLDMS-PTC methods have discovered reasonable CT values, and the COADL-MIAPCD algorithms exhibit higher performance with a minimum CT of 0.51s.

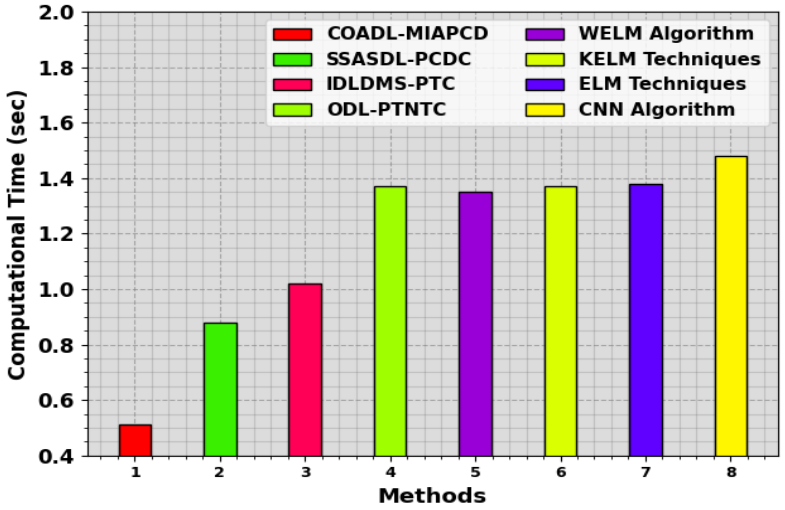

Figure 9. CT Outcome of the COADL-MIAPCD method with other algorithms

Thus, the COADL-MIAPCD technique has been executed for an automated and accurate detection process.

5. Conclusion

In this study, we have introduced a novel COADL-MIAPCD system. The main objective of the COADL-MIAPCD algorithm is to proficiently explore the medical images for the identification of the PC. The COADL-MIAPCD technique primarily applies the MF approach for image pre-processing. In addition, the COADL-MIAPCD technique allowed using of an improved SE-ResNet. Moreover, the COA can be utilized for the optimal parameter choice of the improved SE-ResNet. At last, the ELM classifier has been used for the detection and classification of PCs. The experimental outcomes of the COADL-MIAPCD methodology have been validated using a medical image data. The obtained experimental outcomes implied that the COADL-MIAPCD achieves optimum performance than other approaches.

Acknowledgment: "The author extends her appreciation to Umm Al-Qura University, Saudi Arabia, for funding this research work through Grant Number 25UQU4320372GSSR01R"

Funding: "This research was funded by Umm Al-Qura University, Saudi Arabia, under Grant Number 25UQU4320372GSSR01R"

Conflicts of Interest: "The authors declare no conflict of interest."

References

[1] C. Park, M. D. Rouzi, M. M. U. Atique, M. G. Finco, R. K. Mishra, G. Barba-Villalobos, E. Crossman, C. Amushie, J. Nguyen, C. Calarge, and B. Najafi, "Machine learning-based aggression detection in children with ADHD using sensor-based physical activity monitoring," *Sensors*, vol. 23, no. 10, p. 4949, May 2023.

DOI: https://doi.org/10.54216/FPA.190119
Received: November 02, 2024 Revised: January 09, 2025 Accepted: February 05, 2025

[2] F. Wang, C. Cheng, W. Cao, Z. Wu, H. Wang, W. Wei, Z. Yan, and Z. Liu, "MFCNet: A multi-modal fusion and calibration networks for 3D pancreas tumor segmentation on PET-CT images," *Comput. Biol. Med.*, vol. 155, Mar. 2023, Art. no. 106657.

[3] K. V. Chaithanyadas and G. R. G. King, "Detection of pancreatic tumor from computer tomography images using 3D convolutional neural network," in *Computational Vision and Bio-Inspired Computing*, Singapore: Springer, 2023, pp. 289–303.

[4] K. Sekaran, P. Chandana, N. M. Krishna, and S. Kadry, "Deep learning convolutional neural network (CNN) with Gaussian mixture model for predicting pancreatic cancer," *Multimedia Tools Appl.*, vol. 79, nos. 15–16, pp. 10233–10247, Apr. 2020.

[5] S. Li, J. Xiao, L. He, X. Peng, and X. Yuan, "The tumor target segmentation of nasopharyngeal cancer in CT images based on deep learning methods," *Technol. Cancer Res. Treatment*, vol. 18, Jan. 2019, Art. no. 153303381988456.

[6] A. Gupta, A. Koul, and Y. Kumar, "Pancreatic cancer detection using machine and deep learning techniques," in *Proc. 2nd Int. Conf. Innov. Practices Technol. Manage. (ICIPTM)*, vol. 2, Feb. 2022, pp. 151–155.

[7] S.-L. Liu, S. Li, Y.-T. Guo, Y.-P. Zhou, Z.-D. Zhang, S. Li, and Y. Lu, "Establishment and application of an artificial intelligence diagnosis system for pancreatic cancer with a faster region-based convolutional neural network," *Chin. Med. J.*, vol. 132, no. 23, pp. 2795–2803, Dec. 2019.

[8] M. N. M. Sehmi, M. F. A. Fauzi, W. S. H. M. W. Ahmad, and E. W. L. Chan, "Pancreatic cancer grading in pathological images using deep learning convolutional neural networks," *FResearch*, vol. 10, p. 1057, Nov. 2022.

[9] S.-H. Zhen, M. Cheng, Y.-B. Tao, Y.-F. Wang, S. Juengpanich, Z.-Y. Jiang, Y.-K. Jiang, Y.-Y. Yan, W. Lu, J.-M. Lue, J.-H. Qian, Z.-Y. Wu, J.-H. Sun, H. Lin, and X.-J. Cai, "Deep learning for accurate diagnosis of liver tumor based on magnetic resonance imaging and clinical data," *Frontiers Oncol.*, vol. 10, p. 680, May 2020.

[10] R. Yang, Y. Chen, G. Sa, K. Li, H. Hu, J. Zhou, Q. Guan, and F. Chen, "CT classification model of pancreatic serous cystic neoplasms and mucinous cystic neoplasms based on a deep neural network," *Abdominal Radiol.*, vol. 47, pp. 232–241, Oct. 2021.

[11] E. Yang, J. H. Kim, J. H. Min, W. K. Jeong, J. A. Hwang, J. H. Lee, J. Shin, H. Kim, S. E. Lee, and S. Y. Baek, "nnU-Net-Based Pancreas Segmentation and Volume Measurement on CT Imaging in Patients with Pancreatic Cancer," *Academic Radiology*, 2024.

[12] T. Vaiyapuri, A. K. Dutta, I. H. Punithavathi, P. Duraipandy, S. S. Alotaibi, H. Alsolai, A. Mohamed, and H. Mahgoub, "Intelligent deep-learning-enabled decision-making medical system for pancreatic tumor classification on CT images," *Healthcare*, vol. 10, no. 4, p. 677, Apr. 2022.

[13] J. V. N. Ramesh, T. Abirami, T. Gopalakrishnan, K. Narayanasamy, M. K. Ishak, F. K. Karim, S. M. Mostafa, and A. Allakany, "Sparrow Search Algorithm With Stacked Deep Learning Based Medical Image Analysis for Pancreatic Cancer Detection and Classification," *IEEE Access*, vol. 11, pp. 111927-111935, 2023.

[14] K. Laxminarayanamma, R. V. Krishnaiah, and P. Sammulal, "IDRCNN: A Novel Deep Learning Network Model for Pancreatic Ductal Adenocarcinoma Detection on Computed Tomography," *Int. J. Electr. Comput. Eng. Syst.*, vol. 15, no. 1, pp. 1-11, 2024.

[15] P. Paithane and S. Kakarwal, "LMNS-Net: Lightweight Multiscale Novel Semantic-Net deep learning approach used for automatic pancreas image segmentation in CT scan images," *Expert Syst. Appl.*, vol. 234, p. 121064, 2023.

[16] T. Zhang, Y. Feng, Y. Zhao, Y. Lei, N. Ying, F. Song, Y. He, Z. Yan, Y. Feng, A. Yang, and G. Zhang, "SI-ViT: Shuffle instance-based Vision Transformer for pancreatic cancer ROSE image classification," *Comput. Methods Programs Biomed*, vol. 244, p. 107969, 2024.

[17] A. Lakkshmanan and C. A. Ananth, "An automated deep learning based pancreatic tumor diagnosis and classification model using computed tomography images," *Int. J. Intell. Comput. Cybern.*, vol. 15, no. 3, pp. 454-470, 2022.

DOI: https://doi.org/10.54216/FPA.190119
Received: November 02, 2024 Revised: January 09, 2025 Accepted: February 05, 2025

[18] X. Qin, M. Zhang, C. Zhou, T. Ran, Y. Pan, Y. Deng, X. Xie, Y. Zhang, T. Gong, B. Zhang, and L. Zhang, "A deep learning model using hyperspectral image for EUS-FNA cytology diagnosis in pancreatic ductal adenocarcinoma," *Cancer Med.*, vol. 12, no. 16, pp. 17005-17017, 2023.

[19] P. Choppala, J. S. Meka, and P. P. Reddy, "Isolated Vector Median Filtering for Noise Reduction in Digital Color Images," *Int. J. Adv. Sci. Technol.*, vol. 29, no. 6, pp. 8305-8317, 2020.

[20] X. Y. Kong, X. S. Zhao, X. H. Sun, P. Wang, Y. Wu, R. Y. Peng, Q. Y. Zhang, Y. Z. Wang, R. Li, Y. H. Yang, and Y. R. Lv, "Classification of Glomerular Pathology Images in Children Using Convolutional Neural Networks with Improved SE-ResNet Module," *Interdiscip. Sci.: Comput. Life Sci.*, vol. 15, no. 4, pp. 602-615, 2023.

[21] W. Gu, J. Liao, and S. Cheng, "Bearing capacity prediction of the concrete pile using tunned ANFIS system," *J. Eng. Appl. Sci.*, vol. 71, no. 1, p. 39, 2024.

[22] M. Nahiduzzaman, M. R. Islam, S. R. Islam, M. O. F. Goni, M. S. Anower, and K. S. Kwak, "Hybrid CNN-SVD based prominent feature extraction for grading diabetic retinopathy," *IEEE Access*, vol. 9, pp. 152261-152274, 2021.

DOI: https://doi.org/10.54216/FPA.190119
Received: November 02, 2024 Revised: January 09, 2025 Accepted: February 05, 2025